ADP-ribosylating and vacuolating cytotoxin of *Mycoplasma pneumoniae* represents unique virulence determinant among bacterial pathogens

T. R. Kannan and Joel B. Baseman*

Department of Microbiology and Immunology, University of Texas Health Science Center, 7703 Floyd Curl Drive, San Antonio, TX 78229

Edited by Stanley Falkow, Stanford University, Stanford, CA, and approved March 2, 2006 (received for review December 12, 2005)

Unlike many bacterial pathogens, *Mycoplasma pneumoniae* is not known to produce classical toxins, and precisely how *M. pneumoniae* injures the respiratory epithelium has remained a mystery for >50 years. Here, we report the identification of a virulence factor (MPN372) possibly responsible for airway cellular damage and other sequelae associated with *M. pneumoniae* infections in humans. We show that *M. pneumoniae* MPN372 encodes a 68-kDa protein that possesses ADP-ribosyltransferase (ART) activity. Within its N terminus, MPN372 contains key amino acids associated with NAD binding and ADP-ribosylating activity, similar to pertussis toxin (PTX) S1 subunit (PTX-S1). Interestingly, MPN372 ADP ribosylates both identical and distinct mammalian proteins when compared with PTX-S1. Remarkably, MPN372 elicits extensive vacuolization and ultimate cell death of mammalian cells, including distinct and progressive patterns of cytopathology in tracheal rings in organ culture that had been previously ascribed to infection with WT virulent *M. pneumoniae*. We observed dramatic seroconversion to MPN372 in patients diagnosed with *M. pneumoniae*-associated pneumonia, indicating that this toxin is synthesized *in vivo* and possesses highly immunogenic epitopes.

ADP ribosylation | community-acquired respiratory distress syndrome toxin | vacuolization

The earliest reports of mycoplasmas as infectious agents in humans appeared in the 1940s (1). Definitive studies in the early 1960s established *Mycoplasma pneumoniae* as the singular cause of cold agglutinin-associated primary atypical pneumonia (2, 3). Today, *M. pneumoniae* is the best known of the human mycoplasmas (4). These bacteria are most unusual, lacking typical cell walls possessed by other prokaryotes, using UGA to encode tryptophan, and requiring cholesterol for growth and maintenance of membrane function and integrity. Much has been learned about the role of *M. pneumoniae* as a respiratory tract pathogen (5). *M. pneumoniae* infections constitute 20–40% of all community-acquired pneumonia and are frequently associated with other airway disorders, such as tracheobronchitis and pharyngitis. Extrapulmonary manifestations, such as hematopoietic, dermatologic, joint, central nervous system, liver, pancreas, kidney, and cardiovascular syndromes are considered sequelae of primary *M. pneumoniae* infections. Also, *M. pneumoniae* has been linked to fulminant disease, with multiorgan involvement (6). Therefore, *M. pneumoniae* causes a wide spectrum of pathologies, with more extensive complications than previously recognized (6), yet no single virulence determinant has been associated with these clinical signs and symptoms. In addition, definitive diagnosis and therapeutic decisions relative to *M. pneumoniae* infections are often delayed or lacking because of the long incubation period (average 1–2 weeks) before clinical symptoms can be observed. Further, direct isolation of *M. pneumoniae* from patients frequently fails, and, when successful, broth or colony growth requires 10–21 days.

The early stages of the *M. pneumoniae*–host interplay revolve around successful mycoplasma colonization of the respiratory tract, facilitated by a specialized mycoplasma tip organelle that mediates surface parasitism (4, 5, 7). This distinct terminus is a complex structure, composed of a network of interactive proteins, designated adhesins, and adherence-accessory proteins (5, 7, 8). In addition, subpopulations of mycoplasma "cytoplasmic" proteins, specifically elongation factor-Tu (EF-Tu) and pyruvate dehydrogenase β subunit (PDH-B), are transferred to *M. pneumoniae* membrane surfaces and selectively bind fibronectin, which further promotes mycoplasma interactions with respiratory mucosa (9). Although mycoplasmas are known primarily as extracellular pathogens, recent sightings of intact mycoplasmas distributed throughout the cytoplasm and perinuclear regions of human cells, along with evidence that mycoplasmas are capable of long-term intracellular survival and replication, provide additional insights into their pathogenic potential (10).

However, the events in *M. pneumoniae* pathogenesis that follow cytadherence are poorly understood, and no mycoplasma products have been identified that exhibit classical toxin-like activities. Therefore, the clinical course of mycoplasma infections in humans is thought to be precipitated by host immune and inflammatory responses, rather than direct cytopathological effects initiated by mycoplasmal cell components. In our search to identify virulence factors of *M. pneumoniae*, we used the human lung-enriched protein, surfactant protein A (SP-A), as "bait" to detect *M. pneumoniae* SP-A-binding proteins. SP-A is synthesized primarily by type II pneumocytes and, to a lesser extent, by nonciliated bronchioalveolar epithelial cells and other cell types (11, 12). SP-A serves a number of diverse functions, including facilitation of tubular myelin formation, reutilization of surfactant phospholipids and proteins, and contribution to innate immunity (13). SP-A affinity chromatography enabled us to identify a prominent 68-kDa *M. pneumoniae*-binding protein, which was subsequently sequenced and identified as MPN372 (14). In this study, we implicate MPN372, which we have designated community-acquired respiratory distress syndrome toxin (CARDS TX), as a virulence factor that exhibits ADP-ribosyltransferase (ART) activity and elicits a distinct pattern of cytopathology in mammalian cells.

Results

Primary Sequence and Conserved Amino Acids of MPN372 (CARDS TX). Primary amino acid sequence alignment revealed homologies between the N terminus of MPN372 and pertussis toxin (PTX) S1 subunit of *Bordetella pertussis* (27% identity over 239 resi-

Conflict of interest statement: No conflicts declared.

This paper was submitted directly (Track II) to the PNAS office.

Abbreviations: CARDS TX, community-acquired respiratory distress syndrome toxin; rCARDS TX, recombinant CARDS TX; ART, ADP-ribosyltransferase; PTX, pertussis toxin; EF-Tu, elongation factor-Tu; PDH-B, pyruvate dehydrogenase β subunit; SP-A, surfactant protein A; CFE, cell-free extract; CPE, cytopathic effect.

Data deposition: The sequences reported in this paper have been deposited in the GenBank database (accession nos. DQ447746–DQ447750).

*To whom correspondence should be addressed. E-mail: baseman@uthscsa.edu.

www.pnas.org/cgi/doi/10.1073/pnas.0510644103

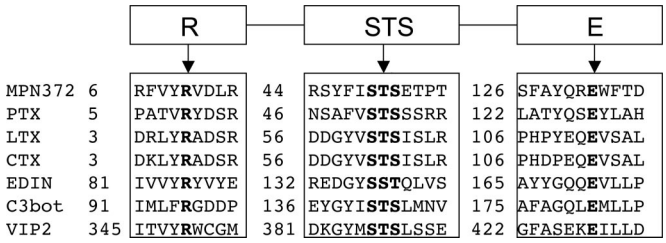

Fig. 1. Alignment of conserved residues between MPN372 and other ARTs. Residues necessary for NAD-binding and catalysis are shown in bold face. PTX, *B. pertussis* pertussis toxin; LTX, *E. coli* heat-labile enterotoxin; CTX, cholera toxin; EDIN, *Staphylococcus aureus* epidermal cell differentiation inhibitor; C3bot, *Clostridium botulinum* C3 toxin; VIP2, *Bacillus cereus* vegetative insecticidal protein.

dues) (14). Although bacterial ADP-ribosylating enzymes do not share extended amino acid conservation, especially relevant in this case was the preservation of three motifs in MPN372 common to bacterial ADP-ribosylating toxins (ADPRTs) (15): (*i*) potential catalytic glutamate as noted by Carroll and Collier (16) observed at position 132; (*ii*) β/α region with a serine-threonine-serine (STS) motif (residing at positions 49 to 51) needed for structural integrity of the NAD-binding site; and (*iii*) conserved arginine residue at position 10 necessary for NAD binding in many ARTs (Fig. 1). Additionally, MPN372 contains histidine 34, which corresponds to His 35 in PTX and His 44 in two other ADP-ribosylating toxins, *Escherichia coli* heat-labile enterotoxin and cholera toxin. As noted earlier, virulence factors, like classical bacterial toxins, have been heretofore undetected among pathogenic mycoplasmas.

Site-Directed Mutagenesis, Expression, and Purification of Recombinant CARDS TX (rCARDS TX). Due to inherent slow growth and modest cell densities of *M. pneumoniae* in complex medium, it is difficult to obtain sufficient amounts of nonabundant mycoplasma proteins to permit functional studies and generate antisera. This hurdle is further complicated by our observation that very little CARDS TX is synthesized in mycoplasma broth cultures. Therefore, it was necessary to express rCARDS TX in *E. coli* to learn more about its biological properties. We used the His-tag expression system and Ni (II)-NTA resin chromatography to generate and purify rCARDS TX protein. Because mycoplasmas use both UGA (universal stop codon) and UGG to encode tryptophan, we analyzed the nucleotide and amino acid sequences of CARDS TX for UGA-encoded tryptophan. The gene encoding CARDS TX possesses eight UGA codons at amino acid positions 148, 195, 233, 364, 392, 450, 462, and 508 that required PCR-mediated, site-directed mutagenesis to replace each UGA codon with UGG to express full-length rCARDS TX (17) (Fig. 2 *Upper*). CARDS TX was predicted to encode a protein of 591 aa. As appears in Fig. 2 *Lower*, the complete CARDS TX gene was cloned, expressed as a His-10-tagged protein and purified to homogeneity.

ART Activity of rCARDS TX. We examined the ability of rCARDS TX to exhibit ART activity in CHO cells because of their sensitivity to PTX activity (18, 19). Non-rCARDS TX-treated CHO cell-free extracts (CFE) possessed weakly radiolabeled protein bands with apparent molecular masses ranging from 26 to ≥50 kDa, indicating normal mono-ADP-ribosylation events that occur via intrinsic CHO-associated ARTs (Fig. 3*a*, lane 1). However, CHO CFE treated with rCARDS TX (Fig. 3*a*, lane 2) possessed additional and intensely radiolabeled ADP-ribosylated proteins with apparent molecular masses of 45, 43, 28, 26, and 21 kDa, reinforcing the ability of CARDS TX to act as an authentic ART. In addition, proteins with molecular

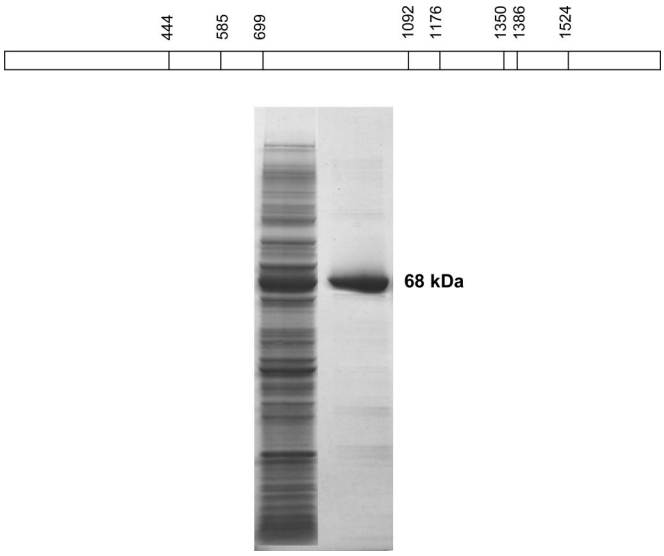

Fig. 2. Expression and purification of CARDS TX protein. (*Upper*) Distribution of UGA codon within *mpn372*. The eight TGA codons within the coding region of CARDS TX were modified into TGG codons (at nucleotide positions shown in the schematic diagram) to express in *E. coli*. (*Lower*) CARDS TX gene was cloned in pET19b vector and expressed in *E. coli* BL21(DE3). Recombinant His-10-tagged protein was purified by using nickel affinity column chromatography and eluted by imidazole. Proteins were resolved in 4–15% gradient SDS/PAGE gel. Lane 1, overexpressed rCARDS TX in *E. coli* BL21(λDE3); lane 2, purified rCARDS TX.

masses ≥90 kDa were ADP-ribosylated (data not shown). We further investigated whether sulfydryl agents influenced rCARDS TX activity. Many bacterial ADP-ribosylating toxins undergo enzymatic activation after reduction of a disulfide bridge, and the primary structure of CARDS TX contains six cysteine residues. Indeed, ADP-ribosylation activity was markedly increased by the presence of DTT (Fig. 3*a*; compare lanes

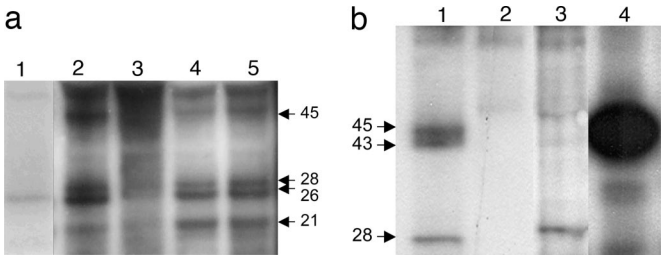

Fig. 3. CARDS TX-mediated ADP ribosylation of mammalian cell proteins. (*a*) ADP ribosylation of CHO cell-free extracts by rCARDS TX. CFEs were prepared from confluent CHO cell monolayers and assayed for ADP ribosylation. CFEs were incubated with and without rCARDS TX. The reaction mixture was precipitated with trichloroacetic acid (TCA), and proteins were resolved by gradient SDS/PAGE and transferred to nitrocellulose membrane for autoradiography as shown. Lanes: 1, CFE alone; 2, CFE + rCARDS TX; 3, CFE + rCARDS TX − DTT; 4, CFE + rCARDS TX − ATP; 5, CFE + rCARDS TX − GTP. (*b*) ADP ribosylation of HEp-2 cell proteins by rCARDS TX or PTX. HEp-2 cell monolayers were incubated with medium alone or in the presence of rCARDS TX or PTX (holotoxin). Cells were washed and incubated with fresh medium, and CFEs were prepared and assayed for ADP ribosylation. The reaction mixture was precipitated with trichloroacetic acid (TCA), and proteins were resolved by SDS/PAGE and transferred to nitrocellulose membrane for autoradiography. Lanes: 1, cells in medium alone followed by preparation of CFE and addition of rCARDS TX; 2, cells pretreated with rCARDS TX followed by preparation of CFE and addition of rCARDS TX; 3, cells pretreated with PTX followed by preparation of CFE and addition of rCARDS TX; 4, cells in medium alone followed by preparation of CFE and addition of PTX.

2 and 3, with and without DTT, respectively), suggesting that rCARDS TX-associated ART activity is sulfhydryl reduction-dependent, similar to cholera and PTXs (20–22). The absence of externally added GTP or ATP revealed less noticeable effects on ADP ribosylation of target proteins (Fig. 3*a*, lanes 4 and 5, respectively).

We further examined rCARDS TX-associated ART activity using human HEp-2 cells as targets (Fig. 3*b*). rCARDS TX-treated HEp-2 CFE contained prominent radiolabeled proteins with apparent molecular masses of 45, 43, 28, 26, and 21 kDa (Fig. 3*b*, lane 1), similar to CHO cell protein patterns observed in Fig. 3*a*, lane 2. When intact and viable HEp-2 cells were preincubated with 5–50 μg of rCARDS TX for 16 h and CFE subsequently prepared and treated with additional rCARDS TX plus [α-^{32}P]NAD, marked decreases in radioactivity of ART-targeted proteins were observed (Fig. 3*b*, lane 2). In other words, HEp-2 cell proteins already modified as a result of their preexposure to rCARDS TX were no longer accessible to ADP ribosylation, further reinforcing rCARDS TX-mediated ADP-ribosylation events. In parallel experiments, similar results were observed in CHO cells. When rCARDS TX was heat-inactivated and added exogenously to intact HEp-2 or CHO cells, rCARDS TX-mediated ADP ribosylation of target proteins in CFE was abolished (data not shown). Importantly, substitution of the CARDS TX-predicted catalytic glutamate (16) at position 132 with alanine (rCARDS TX$^{132glu\rightarrow ala}$) markedly reduced ADP-ribosylation activity, reinforcing the categorization of CARDS TX as a genuine ART-associated bacterial toxin.

To further delineate protein target specificity of ART-related rCARDS TX activity, we compared ADP-ribosylation patterns of rCARDS TX with the S1 subunit of PTX in HEp-2 cells (Fig. 3*b*, lanes 1 and 4). Similarities and differences among ART-targeted proteins were observed. For example, proteins in the range of 25–35 kDa differed between the two toxins whereas other ribosylation patterns seemed to overlap [43 and 45 kDa and $\geq$90 kDa (latter not shown)]. Further, preincubation of intact HEp-2 cells with PTX blocked ADP ribosylation of 45 and 43 kDa proteins, but not of lower molecular mass proteins (ranging from 28–21 kDa) indicating that the latter were subsequently accessible to CARDS TX-mediated ADP ribosylation (Fig. 3*b*, lane 3).

Cytopathic Effects (CPEs) of rCARDS TX on Mammalian Monolayer Cell Cultures. Because we and others reported that mammalian cells parasitized by viable and cytadhering *M. pneumoniae* cells exhibit numerous CPEs due to unknown mycoplasma factors (23), we monitored the effect of rCARDS TX on intact and viable mammalian cells (Fig. 4). CHO cells exposed to exogenous rCARDS TX displayed distinct vacuolization and cell rounding, with disruption of monolayer integrity. Cytopathology was slow to develop at low concentrations of rCARDS TX (10–50 ng/ml), requiring $\approx$24–32 h, whereas higher concentrations of rCARDS TX (10–50 μg/ml; Fig. 4) elicited overt CPE in 6–18 h. Heat inactivation of rCARDS TX preparations (15 min at 100°C) abolished CPE (Fig. 4, control), reinforcing the cytotoxic properties of "heat labile" rCARDS TX and negating the possible contribution of *E. coli* endotoxin in recombinant protein preparations. In the latter case, all recombinant proteins were expressed and purified from lpxM-inactivated *E. coli* BL21 (DE3) (24), which produces a nonmyristylated lipopolysaccharide (nmLPS) with markedly reduced endotoxicity. Also, purified recombinant proteins were passed through sequential polymixin columns to reduce remaining endotoxin contamination before use, and we performed Limulus assays to determine endotoxin concentrations in each recombinant preparation. In all cases, recombinant test samples contained endotoxin levels at or below the minimal detection levels of the assay (0.1 endotoxin units/ml). Only full-length rCARDS TX induced distinct vacuolization of host cell cytoplasm. Interestingly, rCARDS TX$^{132glu\rightarrow ala}$ at 5 μg/ml did not elicit vacuolization in CHO cells; at 25 μg/ml, vacuolization was discernible in only 5–10% of the CHO cell population.

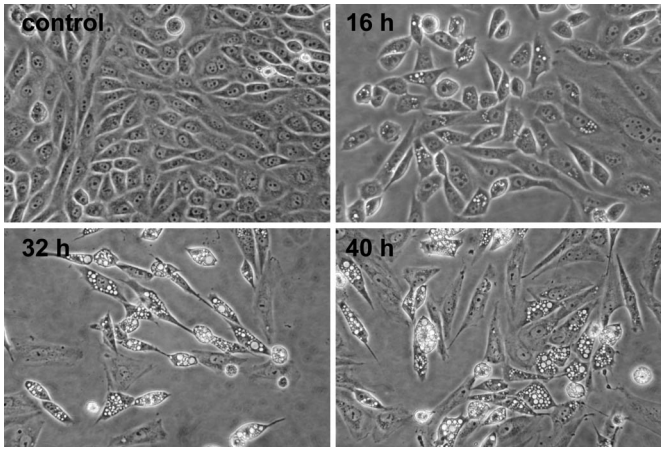

Fig. 4. Effect of rCARDS TX on CHO cell morphology. Cells were grown to 60% monolayer confluence before addition of 10 μg of rCARDS TX for 16–40 h. Control CHO cells were treated with 10 μg of heat-inactivated rCARDS TX for 40 h. (Magnification: $\times$200.)

Intrigued by the vacuolating property of rCARDS TX on CHO cells, we further tested the effect of rCARDS TX on HeLa and HEp2 cells. As observed with CHO cell monolayers, HeLa cells displayed a highly vacuolated phenotype, which was dose- and time-dependent, followed by surface detachment (see Fig. 7, which is published as supporting information on the PNAS web site). HEp-2 cells demonstrated less pronounced CPE. Recombinant *M. pneumoniae* fibronectin-binding proteins rEF-TuMp and rPDH-BMp did not elicit CPE under the same conditions using similar or 10-fold higher molar concentrations.

CPEs of rCARDS TX on Baboon Tracheal Organ Cultures. Baboon tracheal rings retain organized and synchronized ciliary activity and respiratory epithelial integrity for at least 10 days when Hepes-buffered DMEM (pH 7.5) is used as the fluid phase and medium is changed every 2–3 days. However, the addition of 10 μg of rCARDS TX to tracheal rings caused noticeable slowing and asynchronous movement of cilia within 24 h, followed by dramatic reduction or cessation of ciliary movement, cilia disorganization, and possible ciliocytophoria at 48 h. rCARDS TX at 5 and 1.5 μg had similar effects, but the cellular changes were delayed by at least 24–72 h, respectively. Thus, the time required for reduction and disappearance of ciliary activity was CARDS TX dose-dependent. Control cultures, which received similar amounts of heat-inactivated rCARDS TX, exhibited normal ciliary activity and respiratory cellular integrity throughout the duration of the experiment.

To further determine the morphological changes in baboon tracheal rings that accompanied treatment with CARDS TX, we examined parallel tissue sections microscopically. Consistent with reduced ciliary motion, histologic assessment revealed extensive and sequential cytopathological changes, including early events of marked thickening of the epithelial layer due to cellular edema and cytoplasmic vacuolization (Fig. 5), nuclear enlargement with chromatin margination and condensation, disturbance of cellular polarity, disorganization in both airway epithelial and submucosal cells, and foci of pyknotic nuclear fragments. These observations were reinforced by using transmission electron microscopy ($\times$30,000), which revealed dramatic losses of tissue integrity, elimination of ciliated cells and microvilli from respiratory epithelium surfaces, and extensive

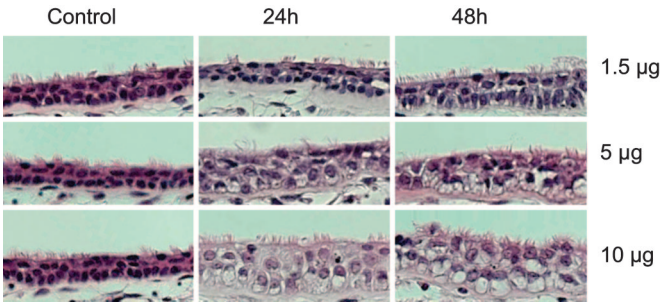

Fig. 5. Effect of rCARDS TX on baboon tracheal epithelium. Baboon tracheal rings were incubated with 1.5, 5, or 10 μg of CARDS TX for 24–48 h in 5 ml of DMEM. Control baboon tracheal rings were treated with heat-inactivated CARDS TX for 48 h. (Magnification: ×200.)

cytoplasmic vacuolization and nuclear fragmentation. These pathological observations suggest a progression of cell injury, degeneration, and death. Thus, within 48–72 h (Fig. 5), extensive disorganization and disruption of respiratory epithelial integrity were evident, responses directly attributable to active CARDS TX and not heat-inactivated preparations.

Does *M. pneumoniae* Secrete CARDS TX? To further determine the location of CARDS TX in *M. pneumoniae* cells (14), we performed SDS/PAGE immunoblot analyses on mycoplasma cell preparations from *M. pneumoniae* clinical isolate S1 and reference strain M129. Whole mycoplasma cell lysates and cytoplasmic, membrane, and culture supernatant fractions obtained from each strain during mid-to-late exponential growth phase were probed by using antiserum raised against rCARDS TX (14). Immunoreactive CARDS TX was detected in total extracts and cytoplasmic and membrane fractions, but not culture supernatants. For example, during late log-phase growth of *M. pneumoniae*, ≈7% of CARDS TX was localized to the mycoplasma membrane (9), with the majority of toxin detected in the cytoplasm. There was no evidence of toxin release into the medium.

Polymorphism in CARDS TX Sequence Among *M. pneumoniae* Clinical Isolates. To establish the presence of CARDS TX in other clinical isolates of *M. pneumoniae*, we characterized three additional strains, designated L2, J1, and RJL1. In each case, CARDS TX was detectable at very low levels by using immunoblot analysis of concentrated mycoplasma cell-associated preparations. Interestingly, when we compared *mpn372* (*cards tx*) gene sequences of reference strain M129 with recent clinical isolates, we observed nucleotide polymorphisms reflected in amino acids at positions 38, 245, 308, 371, 391, and 392. For example, all clinical isolates exhibited changes at amino acid position 371 (Ile to Ser). Only strain JL possessed that single alteration. Strain RJL1 revealed one additional change at position 392 (Trp to Arg). Strain L2 showed one additional change when compared with JL at amino acid position 245 (Asp to Gly). Strain S1 had three additional changes when compared with JL at amino acid positions 38 (Leu to Pro), 308 (Ser to Pro), and 391 (Phe to Ser).

CARDS TX as Immunodominant Target in *M. pneumoniae*-Infected Human. Because rCARDS TX exhibited ART and CPE activities in mammalian cells, thereby displaying bona fide pathogenic determinant characteristics, we screened acute- and convalescent-phase sera of nine documented *M. pneumoniae*-infected individuals for CARDS TX-reactive antibodies. This study would provide direct evidence for the synthesis of CARDS TX during *M. pneumoniae* infection and lend credence to its immunogenic properties and possible diagnostic, prognostic, and vaccinogenic potential. Acute-phase sera, which were obtained at the time of appearance of clinical symptoms, exhibited mild reactivity to rCARDS TX, whereas sequential "convalescent" sera obtained at 14 and 28 days after the initial serum draw demonstrated marked seroconversion to CARDS TX (Fig. 6). Pooled sera from 20 healthy individuals possessed very low reactivity to CARDS TX (Fig. 6, lane C).

Discussion

Mycoplasma pneumoniae causes a wide spectrum of respiratory and extrapulmonary pathologies (4, 6, 25), yet no single identifiable virulence determinant has been associated with these clinical signs and symptoms. Although cytadherence of *M. pneumoniae* to the respiratory tract seems to be the initiating event in the infectious process (26), it is not known how *M. pneumoniae* injures respiratory epithelial cells after colonization (4, 27). For example, it was reported in the 1960s and 1970s that intimate contact and continued biochemical function of *M. pneumoniae* during infection of host respiratory cells was essential for disruption of tissue integrity and cytotoxicity (23, 27–30). These observations and the fact that tracheobronchitis is a common manifestation of *M. pneumoniae* infections are particularly relevant to the studies described here. In those early

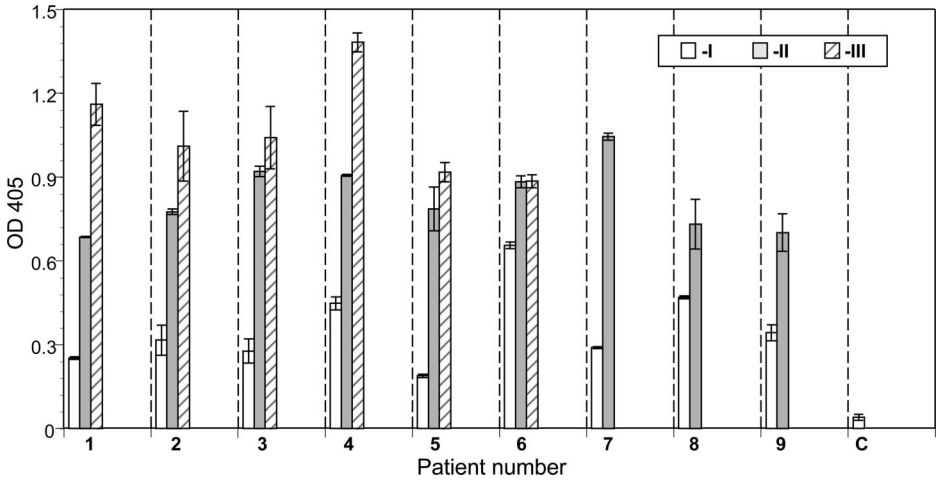

Fig. 6. ELISA-based screening of normal and *M. pneumoniae*-infected individuals for CARDS TX-reactive antibodies. Each well of ELISA plates was coated with rCARDS TX and reacted with patient sera, which were collected at the onset of disease (I) and 14 (II) and 28 (III) days later.

reports, *M. pneumoniae*-infected hamster tracheal organ cultures exhibited decreased rates of macromolecular synthesis, which preceded characteristic ciliostasis and cytoplasmic vacuolization. These events were followed by progressive coalescence of cytoplasmic vacuoles and distortion of the cytoplasm, resulting in extensive cellular fragmentation and sloughing (28, 30–32). Although it was proposed that mycoplasma adherence to host target cells and active mycoplasma metabolic function, including peroxide secretion, contributed to *M. pneumoniae*-mediated pathogenicity (33), no differences in these properties were demonstrable between virulent or attenuated mycoplasmas (28, 34). At that time, we postulated that unknown *M. pneumoniae* "dose-dependent toxic factors" mediated the observed host cell dysfunction and CPE (27). Using tissue culture models and baboon tracheal rings in organ cultures, we have demonstrated that rMPN372 (rCARDS TX) possesses ART activity and elicits characteristic and extensive CPE in mammalian cells. Therefore, our earlier observations in the 1970s have been upheld and extended by the identification of CARDS TX and its ADP-ribosylating and vacuolating properties.

ADP ribosylation involves the transfer of the ADP-ribosyl group from NAD^+ to specific amino acids in target proteins by means of ART activity. Many classical bacterial exotoxins perform this reaction, leading to macromolecular dysfunction, disruption of cellular homeostasis, initiation of CPE, and ultimate cell death (35–37). Although ART-related toxins share limited amino acid conservation within themselves and with CARDS TX, they exhibit conserved catalytic domain-associated amino acids (Fig. 1) (15, 16). Fully expressed rCARDS TX ribosylates specific mammalian host proteins, and ART activity is enhanced in the presence of DTT (Fig. 3*a*). The latter is likely due to protection from oxidation of six cysteine residues that are distributed throughout CARDS TX at positions 240, 257, 324, 406, 425, and 548. Because the predicted ART domain is localized within the first 250 aa, the presence of DTT would maintain the protein in reduced form, which apparently favors ADP ribosylation.

Our data clearly implicate CARDS TX as the cause of vacuolization and CPE in host target cells. Like purified VacA protein of *Helicobacter pylori* (38), rCARDS TX causes the formation of coalescent vacuoles in the cytoplasm of CHO and HeLa cells. Early vacuoles seem to grow in size and fuse with time until the intoxicated cell cytoplasm is occupied by mostly large vacuoles (Fig. 4). Additional results are published in Fig. 7. This process is associated with the progressive addition of membranes, resulting in the alteration of membrane traffic along the endocytic–endosomal pathway (39). Whether a similar mechanism is associated with CARDS TX is unknown. However, the abolition of ADP ribosylation and the dramatic decrease in vacuolization as a result of the CARDS TX glutamate-to-alanine substitution underscore the close relationship between CARDS TX-dependent ART activity, vacuolization, and tissue disorganization. Further, the requirement of close contact between *M. pneumoniae* and respiratory cells to elicit cytopathology (29, 30) is consistent with our observations that a subpopulation of CARDS TX is membrane-associated, trypsin-sensitive, and SP-A-binding (14). Intimate contact between mycoplasma and host cell could result in the release of CARDS TX at membrane–membrane interfaces as well as the introduction of CARDS TX into target cells, leading to ADP ribosylation and vacuolization (Fig. 4). Another possibility is that CARDS TX remains associated with intact mycoplasmas during infection and is released when extracellular mycoplasmas are degraded or viable mycoplasmas invade target cells (10, 40).

Comparisons of *mpn372* sequences among clinical isolates and reference strain M129 revealed one consistent amino acid change ($371^{Ile \rightarrow Ser}$) and several others, as described earlier. It is unclear whether any of these amino acid differences alter CARDS TX activities. However, they may serve to link CARDS TX sequence polymorphisms to epidemiological and pathogenic observations in geographically distinct infected populations.

The fact that patients seroconvert to CARDS TX during *M. pneumoniae* infection is a key observation in implicating CARDS TX as a fundamental virulence determinant because it is clear that CARDS TX is synthesized *in vivo* and is highly immunogenic. It is particularly interesting that a "whoop" has been described frequently in children infected with *M. pneumoniae*, but no mycoplasma-associated factor has ever been correlated with these clinical manifestations. The mode of action of PTX S1 subunit, by means of its ADP-ribosylating properties, directly leads to multiple alterations in protein targets, metabolic pathways, vascular permeability, and inflammation, contributing to the characteristic sound of the whoop in whooping cough (18). Based upon comparative ART profiles (Fig. 3*b*), CARDS TX may elicit toxic activities and clinical symptoms that are both similar to, yet distinguishable from, PTX. In this regard, CARDS TX is the only known ADP-ribosylating toxin discovered among any pathogenic human or animal mycoplasmas and to our knowledge, the only bacterial toxin to display both ADP-ribosylating and vacuolating functions. Because ART bacterial toxins play key roles in pathogenesis and are considered fundamental virulence factors, we hypothesize that the biological properties of CARDS TX relate directly to *M. pneumoniae*-mediated clinical symptoms and pathologies. In other words, we consider CARDS TX to be an authentic pathogenic determinant of *M. pneumoniae*. The long history of *M. pneumoniae* as a very successful bacterial pathogen and its association with characteristic CPE, inflammatory responses, and sequelae that lead to acute and chronic airway diseases and extrapulmonary pathologies are well established (4, 6, 25). Therefore, the detection of this unique ADP-ribosylating and vacuolating toxin in *M. pneumoniae* may help to explain the wide-ranging pathogenic capabilities of *M. pneumoniae* and serve as a diagnostic and prognostic indicator of infection and disease progression as well as a vaccine and anti-drug target.

Materials and Methods

Bacterial Strains and Plasmids. *M. pneumoniae* reference strain M129 and clinical isolates S1 (14), L2, J1, and RJL1; and *E. coli* INV alpha, *E. coli* BL21 (λDE3), and lipid A mutant of *E. coli* BL21 [λDE3, *lpx*M^- (gift from J.-F. Gauchat, University of Montreal, Montreal)] (24) strains were used in this study. Plasmids expressing histidine tag (His-10) recombinant *M. pneumoniae* elongation factor Tu ($rEF\text{-}Tu_{Mp}$) and pyruvate dehydrogenase E1 β subunit ($rPDH\text{-}B_{Mp}$) fusion proteins have been described (9). Plasmids expressing full-length rCARDS TX were constructed by site-directed mutagenesis by using PCR (17) and expressed as His-10-tagged protein by using primers presented in Table 1, which is published as supporting information on the PNAS web site.

Expression and Purification of Recombinant Proteins. Using NdeI and BamHI restriction sites incorporated in the oligonucleotide primers, we cloned the entire fragment containing *mpn372* (or *cards tx*) coding region into *E. coli* His-10-tagged expression vector, pET19b (Novagen) and purified rCARDS TX by nickel and polymixin affinity chromatography (for endotoxin analysis, see *Supporting Materials and Methods*, which is published as supporting information on the PNAS web site). $rCARDS\ TX^{I32glu \rightarrow ala}$ was generated by using PCR-directed site mutagenesis.

Mammalian Cell Lines. Monolayers of CHO-K1, HeLa, and HEp-2 cell (American Type Culture Collection) were grown to 60–75% confluence in 25-ml flasks by using F12-K or MEM media supplemented with 5% FBS. Depleted culture media were replaced by fresh F12-K or MEM without serum but containing

10 ng–50 μg of filter-sterilized (0.22 μm) rCARDS TX, rEF-Tu_{Mp}, or rPDH-B_{Mp}; the latter two served as negative controls. After 2 h at 37°C, 5% FBS was added to each culture and incubation continued for 16–72 h. CHO-K1, HeLa, and HEp-2 cell cultures were observed periodically for morphological changes.

ADP-Ribosylation Assay. ART activity of rCARDS TX was assayed by determining incorporation of [^{32}P]ADP-ribose moiety (from [α-^{32}P]NAD) into indicator mammalian cell proteins as described for PTX (19) (see *Supporting Materials and Methods*).

Baboon Tracheal Organ Cultures. Tracheas from female baboons (8–20 years old) were obtained from the Southwest Foundation for Biomedical Research (San Antonio, TX). Excised tracheas were placed in 50 mM Hepes-buffered DMEM (pH 7.5), supplemented with 100 μg/ml each of penicillin, streptomycin, and gentamycin to control microbial contamination. Tracheal rings of ≈2–3 mm in thickness were prepared by transverse sectioning between each cartilage, and single trachea yielded 14–16 rings with an inner surface lined with ciliated epithelium. Up to three tracheal rings were placed in plastic dishes containing 4.75 ml of medium and incubated overnight at 37°C in 5% CO_2 and air to assess the quality and integrity of individual rings. Ciliary movement was readily discernible through the floor of the plastic dish by using an inverted microscope at ×100 magnification. Between 24 and 48 h after the immersion of tracheal rings in antibiotic-containing medium, 0.25 ml of rCARDS TX (1.5, 5.0, or 10.0 μg/0.25 ml in DMEM) was added; equivalent concentrations of heat-inactivated rCARDS TX were included in control cultures. Histopathology was performed by using standard protocols (see *Supporting Materials and Methods*).

Comparison of CARDS TX Genes Among *M. pneumoniae* Isolates. The entire coding region of CARDS TX was PCR amplified by using primers 1 and 2 (see Table 1) from the chromosomal DNAs of reference strain M129 and clinical isolates with high fidelity Taq polymerase (Sigma-Aldrich), cloned in pCR-II vectors (Invitrogen), and sequenced (Center for Advanced DNA Technologies, University of Texas Health Science Center at San Antonio). Sequences were analyzed by using the BLAST program available in the National Center for Biotechnology Information database (www.ncbi.nlm.nih.gov).

Immune Assessment of *M. pneumoniae*-Infected Patient Sera to rCARDS TX. Acute and convalescent phase sera were collected from patients with *M. pneumoniae*-diagnosed respiratory infections that ranged from tracheobronchitis to bronchopneumonia. These patients were diagnosed with mycoplasma infection based upon >4-fold increases in antibody titers to *M. pneumoniae* by using ELISA and immunoblot criteria and, in some cases, by direct isolation of *M. pneumoniae* from blood. Two or three blood samples were obtained from each patient. The first blood sample was collected during the acute phase of the disease, ≈2 weeks after exposure to *M. pneumoniae*. The second and third serum samples were obtained 14 and 28 days later, respectively. Control baseline serum samples were obtained from healthy women attending the University of Texas Health Science Center at San Antonio Obstetrics and Gynecology Clinic. All serum samples were assessed by immunoblotting against total *M. pneumoniae* proteins and by ELISA for IgG reactivity by using rCARDS TX (see *Supporting Materials and Methods*).

Statistical Analysis. DELTAGRAPH 4 (1999) and Microsoft EXCEL software were used for analyses. Comparison of patients' immune responses was performed with Student's *t* test, and results are presented as means ± SD. The threshold for statistical significance was $P < 0.05$.

We thank Marianna Cagle and Pramod Gowda for technical assistance and Drs. J. J. Coalson, R. L. Reddick, and A. M. Collier for interpretation of histological data. This work was supported by National Institutes of Health Grant AI45737.

1. Eaton, M. D., Meikejohn, G. & Van Herick, W. (1944) *J. Exp. Med.* **79,** 649–667.
2. Couch, R. B., Cate, T. R. & Chanock, R. M. (1964) *J. Am. Med. Assoc.* **187,** 442–447.
3. Feizi, T. & Taylor-Robinson, D. (1967) *Immunology* **13,** 405–409.
4. Baseman, J. B. & Tully, J. G. (1997) *Emerg. Infect. Dis.* **3,** 21–32.
5. Baseman, J. B., Reddy, S. P. & Dallo, S. F. (1996) *Am. J. Respir. Crit. Care Med.* **154,** S137–S144.
6. Waites, K. B. & Talkington, D. F. (2004) *Clin. Microbiol. Rev.* **17,** 697–728.
7. Baseman, J. B. (1993) *Subcell. Biochem.* **20,** 243–259.
8. Krause, D. C. (1996) *Mol. Microbiol.* **20,** 247–253.
9. Dallo, S. F., Kannan, T. R., Blaylock, M. W. & Baseman, J. B. (2002) *Mol. Microbiol.* **46,** 1041–1051.
10. Dallo, S. F. & Baseman, J. B. (2000) *Microb. Pathog.* **29,** 301–309.
11. Balis, J. U., Paterson, J. F., Paciga, J. E., Haller, E. M. & Shelley, S. A. (1985) *Lab. Invest.* **52,** 657–669.
12. Khubchandani, K. R. & Snyder, J. M. (2001) *FASEB J.* **15,** 59–69.
13. Crouch, E. & Wright, J. R. (2001) *Annu. Rev. Physiol.* **63,** 521–554.
14. Kannan, T. R., Provenzano, D., Wright, J. R. & Baseman, J. B. (2005) *Infect. Immun.* **73,** 2828–2834.
15. Domenighini, M. & Rappuoli, R. (1996) *Mol. Microbiol.* **21,** 667–674.
16. Carroll, S. F. & Collier, R. J. (1984) *Proc. Natl. Acad. Sci. USA* **81,** 3307–3311.
17. Ho, S. N., Hunt, H. D., Horton, R. M., Pullen, J. K. & Pease, L. R. (1989) *Gene* **77,** 51–59.
18. Hewlett, E. L., Sauer, K. T., Myers, G. A., Cowell, J. L. & Guerrant, R. L. (1983) *Infect. Immun.* **40,** 1198–1203.
19. Xu, Y. & Barbieri, J. T. (1995) *Infect. Immun.* **63,** 825–832.
20. Moss, J., Stanley, S. J., Morin, J. E. & Dixon, J. E. (1980) *J. Biol. Chem.* **255,** 11085–11087.
21. Mekalanos, J. J., Collier, R. J. & Romig, W. R. (1979) *J. Biol. Chem.* **254,** 5855–5861.
22. Moss, J., Stanley, S. J., Burns, D. L., Hsia, J. A., Yost, D. A., Myers, G. A. & Hewlett, E. L. (1983) *J. Biol. Chem.* **258,** 11879–11882.
23. Hu, P. C., Collier, A. M. & Baseman, J. B. (1976) *Infect. Immun.* **14,** 217–224.
24. Cognet, I., de Coignac, A. B., Magistrelli, G., Jeannin, P., Aubry, J. P., Maisnier-Patin, K., Caron, G., Chevalier, S., Humbert, F., Nguyen, T., *et al.* (2003) *J. Immunol. Methods* **272,** 199–210.
25. Clyde, W. A., Jr. (1979) in *The Mycoplasmas II: Human and Animal Mycoplasmas*, eds. Tully, G. & Whitcomb, R. F. (Academic, New York), Vol. II, pp. 275–306.
26. Baseman, J. B., Cole, R. M., Krause, D. C. & Leith, D. K. (1982) *J. Bacteriol.* **151,** 1514–1522.
27. Hu, P. C., Collier, A. M. & Baseman, J. B. (1975) *Infect. Immun.* **11,** 704–710.
28. Collier, A. M., Clyde, W. A., Jr., & Denny, F. W. (1969) *Proc. Soc. Exp. Biol. Med.* **132,** 1153–1158.
29. Collier, A. M. (1972) in *Pathogenic Mycoplasmas* (Assoc. Sci. Pub., Amsterdam), pp. 307–327.
30. Collier, A. M. & Baseman, J. B. (1973) *Ann. N.Y. Acad. Sci.* **225,** 277–289.
31. Collier, A. M., Clyde, W. A., Jr., & Denny, F. W. (1971) *Proc. Soc. Exp. Biol. Med.* **136,** 569–573.
32. Murphy, G. F., Brody, A. R. & Craighead, J. E. (1980) *Virchows Arch. A Pathol. Anat. Histol.* **389,** 93–102.
33. Tryon, V. V. & Baseman, J. B. (1992) in *Mycoplasmas: Molecular Biology and Pathogenesis*, ed. Maniloff, J. (Am. Soc. Microbiol., Washington, DC), pp. 457–471.
34. Fernald, G. W. (1969) *J. Infect. Dis.* **119,** 255–266.
35. Honjo, T., Nishizuka, Y. & Hayaishi, O. (1968) *J. Biol. Chem.* **243,** 3553–3555.
36. Iglewski, B. H. & Kabat, D. (1975) *Proc. Natl. Acad. Sci. USA* **72,** 2284–2288.
37. Krueger, K. M. & Barbieri, J. T. (1995) *Clin. Microbiol. Rev.* **8,** 34–47.
38. Cover, T. L. & Blaser, M. J. (1992) *J. Biol. Chem.* **267,** 10570–10575.
39. Papini, E., de Bernard, M., Milia, E., Bugnoli, M., Zerial, M., Rappuoli, R. & Montecucco, C. (1994) *Proc. Natl. Acad. Sci. USA* **91,** 9720–9724.
40. Baseman, J. B., Lange, M., Criscimagna, N. L., Giron, J. A. & Thomas, C. A. (1995) *Microb. Pathog.* **19,** 105–116.